Weak capture of protons by protons

R. Schiavilla
Jefferson Lab, Newport News, Virginia 23606
and Department of Physics, Old Dominion University, Norfolk, Virginia 23529

V. G. J. Stoks
Centre for the Subatomic Structure of Matter, University of Adelaide, Adelaide, Australia 5005
and Physics Division, Argonne National Laboratory, Argonne, Illinois 60439

W. Glöckle, H. Kamada,* and A. Nogga
Institut für Theoretische Physik II, Ruhr-Universität Bochum, D-44780 Bochum, Germany

J. Carlson
Theoretical Division, Los Alamos National Laboratory, Los Alamos, New Mexico 87545

R. Machleidt
Department of Physics, University of Idaho, Moscow, Idaho 83483

V. R. Pandharipande
Department of Physics, University of Illinois, Urbana, Illinois 61801

R. B. Wiringa
Physics Division, Argonne National Laboratory, Argonne, Illinois 60439

A. Kievsky
INFN, Sezione di Pisa, I-56100 Pisa, Italy

S. Rosati
Department of Physics, University of Pisa, I-56100 Pisa, Italy
and INFN, Sezione di Pisa, I-56100 Pisa, Italy

M. Viviani
INFN, Sezione di Pisa, I-56100 Pisa, Italy

(Received 2 April 1998)

The cross section for the proton weak capture reaction $^1\mathrm{H}(p,e^+\nu_e)^2\mathrm{H}$ is calculated with wave functions obtained from a number of modern, realistic high-precision interactions. To minimize the uncertainty in the axial two-body current operator, its matrix element has been adjusted to reproduce the measured Gamow-Teller matrix element of tritium β decay in model calculations using trinucleon wave functions from these interactions. A thorough analysis of the ambiguities that this procedure introduces in evaluating the two-body current contribution to the pp capture is given. Its inherent model dependence is in fact found to be very weak. The overlap integral $\Lambda^2(E=0)$ for the pp capture is predicted to be in the range 7.05–7.06, including the axial two-body current contribution, for all interactions considered. [S0556-2813(98)06908-8]

PACS number(s): 21.30.−x, 21.45.+v, 25.10.+s, 95.30.Cq

I. INTRODUCTION

The proton weak capture on protons is the most fundamental process in stellar nucleosynthesis: it is the first reaction in the pp chain converting hydrogen into helium, and the principal source for the production of energy and neutrinos in main-sequence stars. The theoretical description of this hydrogen-burning reaction, whose cross section cannot be measured in terrestrial laboratories, was first given by Bethe and Critchfield [1], who showed that the associated rate was large enough to account for the energy released by the Sun. Since then, a series of calculations has refined their original estimate by either computing the required wave functions more accurately [2–5] or by using more realistic models for the nuclear transition operator [6–8]. We here contribute to this effort by providing an integrated study of these two aspects with emphasis on a reliable estimate of their associated theoretical uncertainties.

This paper is divided into seven sections and an appendix. In Sec. II we set up the framework for the present study, by providing expressions for the pp fusion cross section and the

*Also Institut für Kernphysik, Technische Hochschule Darmstadt, D-64289 Darmstadt, Germany.

required matrix elements and by summarizing the current ''best'' values for the various coupling constants, Fermi function, etc. In Secs. III and IV we give a fairly detailed description of, respectively, the pp and deuteron wave functions, as obtained from modern (high-precision) interactions. The latter include, along with the short-range nuclear part, a complete treatment of electromagnetic effects up to order α^2, α being the fine-structure constant, and accurately reproduce the measured low-energy pp scattering parameters and deuteron properties. Sections V and VI deal with the calculation of the pp cross section in the approximations, respectively, in which only the one-body or both the one- and two-body parts of the axial current operator are retained. In Sec. VI we also review the evidence, as obtained from an analysis of tritium β decay, for the axial two-body components (explicit expressions for them are listed in the Appendix). Because of their model dependence, we adopt the phenomenological approach of adjusting the cutoff masses in the meson-nucleon vertices and N to Δ axial coupling constant so as to obtain agreement with the experimental value for the Gamow-Teller matrix element in tritium β decay. The question of how this procedure impacts the pp cross section is also examined. Finally, in Sec. VII we summarize our conclusions, and provide our ''best'' value for the pp overlap integral at zero energy.

II. CROSS SECTION

The spin-averaged total cross section for the $^1\mathrm{H}(p,e^+\nu_e)^2\mathrm{H}$ reaction can be written in the form [8]

$$\sigma(E)=\frac{1}{(2\pi)^3}\frac{G_V^2}{v_{\mathrm{rel,n.r.}}}m_e^5 f(E)\sum_M |\langle d,M|\mathbf{A}_-|pp\rangle|^2. \tag{2.1}$$

Here G_V is the vector coupling constant for which the value $G_V=(1.149\,39\pm 0.000\,65)\times 10^{-5}$ GeV^{-2}, as obtained from a recent analysis of ft values for superallowed $0^+\to 0^+$ transitions [9], is used; m_e is the electron mass and $v_{\mathrm{rel,n.r.}}$ is the pp relative velocity. The process is induced by the axial-vector part of the weak interaction Hamiltonian, and consequently only even parity pp states contribute to the matrix element.

The naive expression for the Fermi function $f(E)$ is given by

$$f(E)\equiv\frac{1}{m_e^5}\int \delta(E+\Delta m-E_\nu-E_e)p_e E_e E_\nu^2 dE_e dE_\nu$$
$$=\int_1^{(E+\Delta m)/m_e} dx\, x\sqrt{x^2-1}\left(\frac{E+\Delta m}{m_e}-x\right)^2, \tag{2.2}$$

where $\Delta m=2m_p-m_d=0.931\,25$ MeV [10] (m_p and m_d are the proton and deuteron masses, respectively), $E=k^2/m_p$ is the c.m. incident energy, and the energy of the recoiling deuteron is neglected. A more refined treatment of the phase-space factor includes the effect of Coulomb focusing of the emitted e^+ wave function [3] as well as radiative corrections to the cross section. The latter have not actually been calculated for the present reaction but have been estimated to be comparable to those obtained for neutron decay [11]. As a result, the Fermi function is parametrized as

$$f(E)=0.144(1+9.04E), \tag{2.3}$$

with E expressed in MeV. At $E=0$ the expression in Eq. (2.2) gives 0.148, which is about 3% larger than the more accurate estimate from Eq. (2.3).

The deuteron and even parity pp wave functions are written as

$$\Psi_d^M(\mathbf{r})=\left[\frac{u(r)}{r}\mathcal{Y}_{01}^{1M}(\hat{\mathbf{r}})+\frac{w(r)}{r}\mathcal{Y}_{21}^{1M}(\hat{\mathbf{r}})\right]\zeta_0^0, \tag{2.4}$$

$$\psi_{\mathbf{k}}^{(+)}(\mathbf{r})=4\pi\sqrt{2}\sum_{L\,\mathrm{even}}\sum_{M_L} \mathrm{i}^L Y_{LM_L}^*(\hat{\mathbf{k}})\,\frac{e^{\mathrm{i}\delta_L}}{kr}\chi_L(r;k)$$
$$\times Y_{LM_L}(\hat{\mathbf{r}})\,\eta_0^0\zeta_1^1, \tag{2.5}$$

where $\mathcal{Y}_{LS}^{JM}(\hat{\mathbf{r}})$ are the normalized eigenfunctions of the two-nucleon orbital angular momentum L, spin S, and total angular momentum J with projection M; $\eta_S^{M_S}$ and $\zeta_T^{M_T}$ denote, respectively, the eigenstates of the spin S and isospin T with projections M_S and M_T. The deuteron $u(r)$ and $w(r)$, and pp $\chi_L(r;k)$ radial wave functions are obtained from solutions of a Schrödinger equation with nuclear and electromagnetic interactions, the latter including corrections from vacuum polarization, magnetic moment, two-photon exchange, and Darwin-Foldy terms. A discussion of the interactions and radial wave functions is given in Secs. III and IV below. Here, it suffices to say that $\chi_L(r;k)$ behaves asymptotically as

$$\chi_L(r;k)\underset{r\to\infty}{\sim}\cos\,\delta_L F_L(kr)+\sin\,\delta_L G_L(kr), \tag{2.6}$$

where δ_L is the phase shift, and F_L and G_L are the regular and irregular Coulomb functions.

The nuclear axial current operator consists of one- and two-body components

$$\mathbf{A}_a=\mathbf{A}_a^{(1)}+\mathbf{A}_a^{(2)}, \tag{2.7}$$

where $a=\pm$ is an isospin index, and

$$\mathbf{A}_\pm^{(1)}=-g_A\sum_i \boldsymbol{\sigma}_i\tau_{i,\pm}, \tag{2.8}$$

$$\tau_{i,\pm}=(\tau_{i,x}\pm\mathrm{i}\tau_{i,y})/2. \tag{2.9}$$

The ratio of the axial to vector coupling constants, $g_A=G_A/G_V$, is taken to be [11] 1.2654 ± 0.0042 by averaging values obtained, respectively, from the beta asymmetry in the decay of polarized neutrons (1.2626 ± 0.0033) [12,13], and $ft(n)$ and $ft(0^+\to 0^+)$, and $g_A=[2ft(0^+\to 0^+)/ft(n)-1]/3=1.2681\pm 0.0033$ [11]. The form of the axial two-body current operator depends on the dynamical model used to construct it. However, the need for such a term is based on an analysis of tritium β decay. This evidence as well as the impact of the ambiguities associated with the form of $\mathbf{A}^{(2)}$ on the pp fusion cross section is discussed below in Sec. VI.

Selection rules for a vector operator restrict the sum over L in the initial capture state, Eq. (2.5), to the values $L=0$ and 2. However, the $L=2$ contribution is negligible at very low energies. Indeed, the initial S- and D-wave channel contributions to the matrix element of the dominant $\mathbf{A}^{(1)}$ operator are proportional to, respectively,

$$\int_0^\infty dr\ u(r)\chi_0(r;k) \simeq \int_0^\infty dr\, u(r)F_0(kr), \tag{2.10}$$

$$\int_0^\infty dr\, w(r)\chi_2(r;k) \simeq \int_0^\infty dr\, w(r)F_2(kr), \tag{2.11}$$

where the $\chi_L(r;k)$ radial wave functions have been replaced with their asymptotic forms by setting $\delta_L \simeq 0$, which is appropriate for the energy range under consideration here (a few keV). It is then easily seen that

$$\frac{\int_0^\infty dr\, w(r)F_2(kr)}{\int_0^\infty dr\, u(r)F_0(kr)} \simeq 2\sqrt{\left(1+\frac{1}{\bar{\eta}^2}\right)\left(1+\frac{1}{4\bar{\eta}^2}\right)} \times \frac{\int_0^\infty dr\sqrt{r}w(r)I_5(2\sqrt{\alpha m_p r})}{\int_0^\infty dr\sqrt{r}u(r)I_1(2\sqrt{\alpha m_p r})}, \tag{2.12}$$

where $\bar{\eta}=\alpha/v_{\text{rel,n.r.}}$, I_L are modified Bessel functions, and the asymptotic expressions, valid in the regime where $\bar{\eta} \gg kr$, have been used for the F_L [14]. The ratio above is found to be roughly 0.000 13 in the limit $v_{\text{rel,n.r.}} \to 0$ (corresponding to $\bar{\eta} \to \infty$).

Finally, the dependence of $\mathbf{A}_a$ upon the momentum transfer $\mathbf{q}=-\mathbf{p}_e-\mathbf{p}_\nu$, where $\mathbf{p}_e$ and $\mathbf{p}_\nu$ are the outgoing lepton momenta, is ignored in Eq. (2.8), because of the very low energies involved. At $E=0$ the kinetic energy available to the final state is only about 420 keV, and the finite momentum transfer correction to the matrix element of $\mathbf{A}^{(1)}$ for S-wave capture can be estimated to be approximately $(qr_d)^2 \simeq (0.0042)^2$, where $q \simeq 420$ keV and $r_d \simeq 2$ fm is the root-mean-square radius of the deuteron—a tiny correction, indeed.

III. *pp* WAVE FUNCTION

The low-energy pp scattering is described by the radial Schrödinger equation

$$\left[\frac{d^2}{dr^2}+k^2-\frac{L(L+1)}{r^2}-m_p V(r)\right]\chi_L(r;k)=0, \tag{3.1}$$

with $\chi_L(r;k)$ the radial wave function, m_p the proton mass, and L the orbital angular momentum. The c.m. relative momentum k is given by $k^2=m_p T_{\text{lab}}/2$. The boundary conditions for the wave function are

$$\chi_L(0;k)=0,$$

$$\chi_L(r;k) \underset{r\to\infty}{\sim} F_L(kr)C_1+G_L(kr)C_2, \tag{3.2}$$

with F_L and G_L the standard regular and irregular Coulomb functions [14]. The potential $V(r)$ can be divided into a long-range electromagnetic part V_{EM} and a short-range nuclear part V_N. The coefficients C_1 and C_2 contain all the necessary information about the partial wave, which is usually expressed in terms of the phase shift δ^C:

$$\tan\delta^C = C_2 C_1^{-1}. \tag{3.3}$$

In a practical calculation, the Schrödinger equation (3.1) is integrated out to some r, large in comparison with the range of the short-range (i.e., nuclear) force. The numerical wave function is then matched to the asymptotic form of Eq. (3.2), and the corresponding phase shift is defined to be the phase shift of the nuclear force with respect to Coulomb wave functions. Following the notation of Ref. [15], we have added the superscript C, for Coulomb.

However, in reality the electromagnetic interaction in pp scattering is much more complicated than just the simple Coulomb interaction. This leads to some practical problems in applying the scenario of integrating the Schrödinger equation, matching to Coulomb functions, and extracting the phase shift. This will be discussed below.

The full interaction, up to second order in the fine-structure constant $\alpha \approx 1/137$, is given by [15–17]

$$V_{\text{EM}}(pp)=V_{C1}+V_{C2}+V_{\text{VP}}+V_{\text{MM}}+V_{\text{DF}}, \tag{3.4}$$

where

$$V_{C1}=\alpha'\frac{F_C(r)}{r}, \tag{3.5}$$

$$V_{C2}=-\frac{\alpha}{2m_p^2}\left[(\Delta+k^2)\frac{F_C(r)}{r}+\frac{F_C(r)}{r}(\Delta+k^2)\right] \approx -\frac{\alpha\alpha'}{m_p}\left[\frac{F_C(r)}{r}\right]^2, \tag{3.6}$$

$$V_{\text{VP}}=\frac{2\alpha}{3\pi}\frac{\alpha'}{r}I_{\text{VP}}(r), \tag{3.7}$$

$$V_{\text{MM}}=-\frac{\alpha}{4m_p^2}\mu_p^2\left[\frac{2}{3}F_\delta(r)\boldsymbol{\sigma}_1\cdot\boldsymbol{\sigma}_2+\frac{F_t(r)}{r^3}S_{12}\right] -\frac{\alpha}{2m_p^2}(4\mu_p-1)\frac{F_{ls}(r)}{r^3}\mathbf{L}\cdot\mathbf{S}, \tag{3.8}$$

$$V_{\text{DF}}=-\frac{\alpha}{4m_p^2}F_\delta(r). \tag{3.9}$$

Here the $F_C(r)$, $F_\delta(r)$, $F_t(r)$, and $F_{ls}(r)$ are functions representing the finite size of the nucleon charge distribution. In the limit of point nucleons, $F_C(r)=F_t(r)=F_{ls}(r)=1$,

whereas $F_\delta(r)=4\pi\delta^3(\mathbf{r})$. Their explicit r dependence is given in Ref. [16]. The various contributions are described as follows.

The Coulomb interaction V_{C1} contains a well-known [18] energy dependence through $\alpha'=2k\alpha/(m_p v_{\rm lab})$. However, at the extreme low energies of interest to astrophysical calculations (a few keV), this energy dependence is negligible, and we can set $\alpha'=\alpha$ for all practical purposes.

The two-photon-exchange interaction V_{C2} behaves like $1/r^2$, and so we immediately have the problem that, in principle, we have to integrate out to infinitely large distances before we can match to Coulomb functions.

The vacuum polarization potential $V_{\rm VP}$ describes the augmentation of the photon propagator by an electron-positron pair. In the limit of point protons $[F_C(r)=1]$, the vacuum polarization integral is given by [19]

$$I_{\rm VP}(r)=\int_1^\infty dx\, e^{-2m_e rx}\left(1+\frac{1}{2x^2}\right)\frac{(x^2-1)^{1/2}}{x^2}, \quad (3.10)$$

with $m_e=0.511$ MeV the electron mass. Including the finite-size effect, we get the more complicated expression as given by Bohannon and Heller [17], where the exponential is replaced by

$$\begin{aligned} e^{-2m_e rx}\rightarrow & D^4(x)e^{-2m_e rx} \\ & -\left[D^4(x)+\frac{1}{2}\rho D^3(x)+\frac{1}{8}(\rho+\rho^2)D^2(x)\right. \\ & \left.+\frac{1}{48}(3\rho+3\rho^2+\rho^3)D(x)\right]e^{-\rho}, \end{aligned} \quad (3.11)$$

where $\rho=br$, $D(x)=[1-(2m_e x/b)^2]^{-1}$, and $b=4.27$ fm^{-1}. As a matter of fact, the simple multiplication of Eq. (3.10) with $F_C(r)$ as an approximation to the inclusion of finite-size effects (and which was adopted in Ref. [16]) already closely resembles the exact treatment (3.11) where the finite-size effect is properly folded into the integral.

The magnetic moment interaction $V_{\rm MM}$ arises as a consequence of the nonvanishing value of the proton magnetic moment, $\mu_p=2.792\,85\mu_0$, while the Darwin-Foldy term $V_{\rm DF}$ is a short-range potential, describing the finite size of the proton, where $F_\delta(r)\rightarrow 4\pi\delta^3(\mathbf{r})$ in the limit of point protons.

Now that we have defined the full long-range electromagnetic interaction, we can return to the question of how, in practice, to integrate the Schrödinger equation and extract the phase shift. We will restrict ourselves to S waves, and so the tensor and spin-orbit terms in the magnetic moment interaction vanish. It is convenient to define a phase shift δ_W^V, which is the phase shift of the solution of the potential W with respect to the solution with the potential V as the interaction. The well-known application of this procedure is the situation where V is the Coulomb potential and W is the Coulomb plus nuclear potential, and the phase shift $\delta_N=\delta_{C+N}^C$ is obtained by matching the numerical solution to Coulomb wave functions as in Eq. (3.2).

If we are to include V_{C2} in W, we run into the problem that we have to integrate out to infinitely large distances before we can match to Coulomb functions. However, by including the point-nucleon limit of V_{C2} also in V, the asymptotic wave function can be expressed in terms of noninteger L' Coulomb functions, where L' satisfies

$$L'(L'+1)=L(L+1)-\alpha\alpha'. \quad (3.12)$$

The asymptotic behavior of the wave function is now given by

$$\chi_L(r)\sim\tilde{F}_L(kr)C_1+\tilde{G}_L(kr)C_2, \quad (3.13)$$

with $\tilde{F}_L(kr)=F_{L'}(kr)$ and similarly for $\tilde{G}_L(kr)$. The advantage is clear immediately: we only have to integrate out to distances large with respect to the nuclear interaction, which is only about 20 fm. But we have to bear in mind that now the phase shift is $\delta_{C1+C2+{\rm FS}+N}^{C1+C2}$, where it should be understood implicitly that the superscript refers to the interactions in the point-nucleon limit, while the interaction denoted by the subscript includes also the (short-range) finite-size effects. To make this clear explicitly, we have here separated off the finite-size effects by writing them symbolically as being due to some short-range potential $V_{\rm FS}$. In this notation, the phase shift with respect to Coulomb functions, as defined in Eq. (3.3), now reads

$$\begin{aligned} \delta^{C1}&=\delta_{C1+C2+{\rm FS}+N}^{C1}=\delta_{C1+C2+{\rm FS}+N}^{C1+C2}+\delta_{C1+C2}^{C1} \\ &=\delta_{C1+C2+{\rm FS}+N}^{C1+C2}+\rho_L, \end{aligned} \quad (3.14)$$

where ρ_L can be easily expressed in terms of the standard Coulomb phase shift σ_L as

$$\rho_L=\sigma_{L'}-\sigma_L-(L'-L)\pi/2. \quad (3.15)$$

The next step is to also include the vacuum polarization. The case where we only have the Coulomb and vacuum polarization has been discussed in detail by Durand [20] and Heller [21], who derive expressions for the relevant asymptotic wave functions and vacuum polarization phase shift $\tau_L\equiv\delta_{C1+{\rm VP}}^{C1}$. Although the vacuum polarization potential exhibits an exponential falloff, the small value of the electron mass means that the Schrödinger equation has to be integrated out to several hundred Fermi before the potential has dropped to sufficiently small values, and it is only then that the numerical solution can be properly matched to the asymptotic solution.

The presence of V_{C2} considerably worsens the situation. Since the $1/r^2$ behavior of V_{C2} is of longer range than the exponential decay of $V_{\rm VP}$, the Schrödinger equation has to be integrated out to distances where $V_{\rm VP}$ is negligibly small as compared to V_{C2}. It is only then that we can match the numerical solution to the proper asymptotic solution and define the phase shift. Unfortunately, because of the slow falloff of the vacuum polarization and the small magnitude of the two-photon-exchange contribution, we now have to integrate out to much larger distances. Even at a distance of 2000 fm the vacuum polarization has only dropped to about 1% of the two-photon exchange.

The scenario of getting the pp wave function for a particular nuclear interaction V_N in the S wave in the presence of the full electromagnetic interaction $V_{\rm EM}$ is now as follows. We integrate the Schrödinger equation out to a distance of

3000 fm, where the numerical solution is matched to the electromagnetic wave functions $\overline{F}_0(kr)$ and $\overline{G}_0(kr)$. The latter are defined to be the solutions of the Schrödinger equation in the presence of the point-nucleon $C1+C2+\mathrm{VP}$ interaction. This procedure, therefore, determines the phase shift δ^{EM} of the nuclear plus full electromagnetic interaction with respect to the point-nucleon $C1+C2+\mathrm{VP}$ interaction. It should be stressed that this phase shift is *not* the same as the phase shift of the nuclear interaction in the presence of only the Coulomb interaction (δ^C_{C+N}). The relation between these electromagnetic wave functions and the standard Coulomb wave functions $F_0(kr)$ and $G_0(kr)$ is given by

$$\begin{pmatrix} \overline{F}_0 \\ \overline{G}_0 \end{pmatrix} = \begin{pmatrix} \cos(\rho_0+\tau_0') & \sin(\rho_0+\tau_0') \\ -\sin(\rho_0+\tau_0') & \cos(\rho_0+\tau_0') \end{pmatrix} \begin{pmatrix} F_0 \\ G_0 \end{pmatrix}, \tag{3.16}$$

with ρ_0 and τ_0' the two-photon-exchange and vacuum polarization S-wave phase shifts, respectively. The prime in the vacuum polarization is to indicate that this is the vacuum polarization phase shift *in the presence of* V_{C2}, which is slightly different from what is defined in Refs. [20,21]. Note that the numerical wave function is now properly normalized as in Eq. (3.2), since $\delta^C=\delta^{\mathrm{EM}}+\rho_0+\tau_0'$.

It should be pointed out that at extreme low energies (a few keV), δ^{EM} is almost zero, and ρ_0 is of the order of a few times 10^{-4} deg, whereas τ_0' rapidly drops from about -10^{-2} deg at 10 keV to -10^{-5} deg at 2 keV, and so δ^C exhibits a change of sign and goes through zero as a function of energy. Hence, it is not recommended to use the normalization as advocated by Kamionkowski and Bahcall in Ref. [5], i.e.,

$$\overline{\chi}_0(r;k) \underset{r\to\infty}{\sim} C_0[G_0(kr)+\cot\delta_0 F_0(kr)], \tag{3.17}$$

with C_0 the Gamow penetration factor. In their case [5], there is no problem (although δ^C is very small and $\cot\delta^C$ becomes very large), because they did not include V_{C2}. Furthermore, with this normalization (3.17), the overlap integral Λ, defined below, requires knowledge of the pp scattering length a_{pp}, where the presence of V_{C2} and V_{VP} in the full electromagnetic interaction defines a rather complicated effective-range function [15]. On the other hand, the normalization (3.2) advocated here allows for an immediate substitution of the numerical wave function (as obtained from solving the Schrödinger equation) into the expression for Λ as defined by Salpeter [2], without having to worry about a phase shift which goes through zero at these extreme low energies and without having to define a complicated effective-range function.

IV. DEUTERON WAVE FUNCTION

The deuteron is the bound state of protons and neutrons in the coupled ${}^3S_1+{}^3D_1$ two-nucleon system. For a given local NN potential $V(\mathbf{r})$, the radial wave functions $u(r)$ and $w(r)$ for the deuteron S and D states, respectively, can be obtained from the coupled Schrödinger equation

$$\left[\frac{d^2}{dr^2}-\gamma^2\right]u(r)=\overline{m}[V_{00}(r)u(r)+V_{02}(r)w(r)],$$

$$\left[\frac{d^2}{dr^2}-\gamma^2-\frac{6}{r^2}\right]w(r)=\overline{m}[V_{20}(r)u(r)+V_{22}(r)w(r)], \tag{4.1}$$

where $\overline{m}$ is twice the reduced mass of proton and neutron, i.e.,

$$\overline{m}\equiv\frac{2m_pm_n}{m_p+m_n}. \tag{4.2}$$

All NN potentials applied in this study use consistently the latest, very accurate, values for nucleon masses [12], namely,

$$m_p=938.272\ 31\ \mathrm{MeV}, \tag{4.3}$$

$$m_n=939.565\ 63\ \mathrm{MeV}, \tag{4.4}$$

implying

$$\overline{m}=938.918\ 52\ \mathrm{MeV}. \tag{4.5}$$

For the NN potential acting in particular partial waves, we have introduced the convenient shorthand notation $V_{00}(r)\equiv\langle{}^3S_1|V|{}^3S_1\rangle$, $V_{02}(r)\equiv\langle{}^3S_1|V|{}^3D_1\rangle$, etc., where $\langle\hat{\mathbf{r}}|{}^3S_1\rangle\equiv\mathcal{Y}_{01}^{1M}(\hat{\mathbf{r}})$ and $\langle\hat{\mathbf{r}}|{}^3D_1\rangle\equiv\mathcal{Y}_{21}^{1M}(\hat{\mathbf{r}})$. The quantity $\gamma=ik$ is discussed below.

The radial wave functions are properly normalized to unity,

$$\int_0^\infty dr[u^2(r)+w^2(r)]=1. \tag{4.6}$$

The asymptotic behavior of the wave functions for large values of r is

$$u(r)\sim A_S e^{-\gamma r},$$

$$w(r)\sim A_D e^{-\gamma r}\left[1+\frac{3}{(\gamma r)}+\frac{3}{(\gamma r)^2}\right], \tag{4.7}$$

where A_S and A_D are known as the asymptotic S- and D-state normalizations, respectively. In addition, one defines the ''D/S-state ratio'' $\eta\equiv A_D/A_S$.

Other deuteron parameters of interest are the quadrupole moment

$$Q_d=\frac{1}{20}\int_0^\infty dr\, r^2 w(r)[\sqrt{8}u(r)-w(r)], \tag{4.8}$$

the root-mean-square or matter radius

$$r_d=\frac{1}{2}\left\{\int_0^\infty dr\, r^2[u^2(r)+w^2(r)]\right\}^{1/2}, \tag{4.9}$$

and the D-state probability

$$P_D = \int_0^\infty dr\, w^2(r). \tag{4.10}$$

Similar to scattering, the deuteron equation, Eq. (4.1), is solved numerically by integrating out to some large r (25 fm in our case) and matching the numerical waves to their asymptotic forms, Eq. (4.7), producing A_S, A_D, and γ from which the predicted deuteron binding energy is extracted.

As mentioned, in the Schrödinger equation, Eq. (4.1), the interaction between the two nucleons is represented by a local potential $V(\mathbf{r})$, with $\mathbf{r}=\mathbf{r}_2-\mathbf{r}_1$ the relative displacement between nucleons 1 and 2. However, in general, the NN potential V is nonlocal, i.e., $V\equiv V(\mathbf{r},\mathbf{r}')$, where $\mathbf{r}$ is the distance between the two ingoing nucleons and $\mathbf{r}'$ the one between the outgoing nucleons. A local potential can then be written as $V(\mathbf{r},\mathbf{r}')|_{\rm local}=\delta(\mathbf{r}-\mathbf{r}')V(\mathbf{r})$. For the more general case of a nonlocal potential, the coupled Schrödinger equation reads

$$\left[\frac{d^2}{dr^2}-\gamma^2\right]u(r)=\overline{m}\int_0^\infty dr'rr'[V_{00}(r,r')u(r') + V_{02}(r,r')w(r')],$$

$$\left[\frac{d^2}{dr^2}-\gamma^2-\frac{6}{r^2}\right]w(r)=\overline{m}\int_0^\infty dr'rr'[V_{20}(r,r')u(r') + V_{22}(r,r')w(r')]. \tag{4.11}$$

This system of coupled integro-differential equations is then solved by a combination of finite-difference, integral-discretization, and matrix-inversion techniques.

Alternatively, one may consider the two-nucleon system in momentum space, where the deuteron wave function is given by

$$\Psi_d^M(\mathbf{q})=[\psi_0(q)\mathcal{Y}_{01}^{1M}(\hat{\mathbf{q}})+\psi_2(q)\mathcal{Y}_{21}^{1M}(\hat{\mathbf{q}})]\zeta_0^0, \tag{4.12}$$

with the normalization

$$\int_0^\infty dq\, q^2[\psi_0^2(q)+\psi_2^2(q)]=1. \tag{4.13}$$

The momentum-space Schrödinger equation that corresponds to Eq. (4.11) consists of two coupled integral equations

$$\psi_0(q)=-\frac{\overline{m}}{\gamma^2+q^2}\int_0^\infty dq'q'^2[V_{00}(q,q')\psi_0(q') + V_{02}(q,q')\psi_2(q')],$$

$$\psi_2(q)=-\frac{\overline{m}}{\gamma^2+q^2}\int_0^\infty dq'q'^2[V_{20}(q,q')\psi_0(q') + V_{22}(q,q')\psi_2(q')]. \tag{4.14}$$

Considering a finite set of discrete arguments for the functions on the left-hand side (LHS) and using the same set of momenta to discretize the integrals on the RHS produces a matrix equation that is solved easily by the matrix-inversion method [22].

The relevant Fourier transforms linking the configuration-space and the momentum-space approaches are

$$V_{LL'}(q,q')=\frac{2}{\pi}\int_0^\infty dr\, r^2 \times\int_0^\infty dr'r'^2 j_L(qr)V_{LL'}(r,r')j_{L'}(q'r'), \tag{4.15}$$

with $V_{LL'}(r,r')|_{\rm local}=\delta(r-r')V_{LL'}(r)/rr'$ if the potential is local and

$$\frac{u_L(r)}{r}=\sqrt{\frac{2}{\pi}}\int_0^\infty dq\, q^2 j_L(qr)\psi_L(q), \tag{4.16}$$

with $u_0(r)\equiv u(r)$, $u_2(r)\equiv w(r)$, and j_L the spherical Bessel functions.

Since high reliability and precision are an important aspect of our present investigation, we have calculated the deuteron wave functions for some local potentials both ways: first, by solving Eq. (4.1) directly and, second, by solving Eq. (4.14) by matrix inversion and then performing the transformation, Eq. (4.16), numerically. We find agreement between the resulting deuteron waves to at least six significant digits for any r in the range 0.05–14 fm. This establishes the reliability of our numerical methods. It also implies that in cases where we use the momentum-space approach and Eq. (4.16), as for the nonlocal potentials, our deuteron waves are of the highest numerical precision.

The deuteron is a pole in the S matrix at $k=i\gamma$. The relativistic relationship between γ and the deuteron binding energy B_d is given by [10]

$$\sqrt{s}=m_d=m_p+m_n-B_d=\sqrt{m_p^2-\gamma^2}+\sqrt{m_n^2-\gamma^2}, \tag{4.17}$$

where m_d denotes the deuteron rest mass. Notice that this equation determines *the correct empirical* γ, since nature is relativistic. We note that in NN scattering we use the relativistic relationship between k and $T_{\rm lab}$, which implies that the c.m. kinetic energy T is related to k according to

$$\sqrt{s}=m_p+m_n+T=\sqrt{m_p^2+k^2}+\sqrt{m_n^2+k^2}. \tag{4.18}$$

Thus, consistency with the scattering problem requires the use of Eq. (4.17) to determine γ. The formal solution of Eq. (4.17) is

$$\gamma^2=[4m_p^2m_n^2-(m_d^2-m_p^2-m_n^2)^2]/4m_d^2, \tag{4.19}$$

and, using $B_d=2.224\,575$ MeV and $\hbar c=197.327\,053$ MeV fm, the accurate numerical value for γ comes out to be

$$\gamma=0.231\,538\,0\ \text{fm}^{-1}. \tag{4.20}$$

To obtain some pedagogical insight into γ^2, one may rewrite Eq. (4.19) in factorized form

$$4m_d^2\gamma^2=[(m_n+m_p)^2-m_d^2][m_d^2-(m_n-m_p)^2]$$
$$=B_d(4m-B_d)(m_d^2-\delta m^2), \tag{4.21}$$

where we introduce the average nucleon mass,

$$m\equiv\frac{m_p+m_n}{2}=938.918\ 97\ \text{MeV}, \tag{4.22}$$

and the nucleon mass difference $\delta m\equiv m_n-m_p=1.293\ 32$ MeV, and used $m_d=2m-B_d$. From this we get

$$\gamma^2=mB_d\left(1-\frac{B_d}{4m}\right)\left(1-\frac{\delta m^2}{m_d^2}\right), \tag{4.23}$$

and rewriting twice the reduced nucleon mass [cf. Eq. (4.2)] in terms of the average mass

$$\overline{m}=m\left(1-\frac{\delta m^2}{4m^2}\right)\ , \tag{4.24}$$

we finally obtain

$$\gamma^2=\overline{m}B_d\left(1-\frac{B_d}{4m}\right)\frac{1-\delta m^2/m_d^2}{1-\delta m^2/(4m^2)}$$
$$\approx\overline{m}B_d\left[1-\frac{B_d}{4m}\left(1-\frac{\delta m^2}{m^2}\right)\right]$$
$$\approx\overline{m}B_d\left(1-\frac{B_d}{4m}\right). \tag{4.25}$$

The approximations involved in Eq. (4.25) are good to 1 part in 10^9. Therefore, this equation reproduces the exact value for γ to all digits given in Eq. (4.20). One can now identify the term $\overline{m}B_d$ as the nonrelativistic approximation to γ^2 and the factor $(1-B_d/4m)$ as the essential relativistic correction. In most calculations of the past, the nonrelativistic γ was used, $\gamma_{\rm nr}\equiv\sqrt{\overline{m}B_d}=0.231\ 606\ 6\ \text{fm}^{-1}$. The difference between $\gamma_{\rm nr}$ and the correct γ, Eq. (4.20), leads to a small difference (0.03%) in the overlap integral Λ^2 (see below). Although the difference is rather small, we believe one should use the relativistically correct value, Eq. (4.20).

Besides the strong interaction, there is also a nonvanishing electromagnetic interaction between protons and neutrons that can be written as [16]

$$V_{\rm EM}(np)=V_{C1}(np)+V_{\rm MM}(np), \tag{4.26}$$

where

$$V_{C1}(np)=\alpha\beta_n\frac{F_{np}(r)}{r},$$

$$V_{\rm MM}(np)=-\frac{\alpha}{4m_pm_n}\mu_p\mu_n\left[\frac{2}{3}F_\delta(r)\boldsymbol{\sigma}_1\cdot\boldsymbol{\sigma}_2+\frac{F_t(r)}{r^3}S_{12}\right]$$
$$-\frac{\alpha}{m_p\overline{m}}\mu_n\frac{F_{ls}(r)}{r^3}(\mathbf{L}\cdot\mathbf{S}+\mathbf{L}\cdot\mathbf{A}). \tag{4.27}$$

Here $\mathbf{A}=(\boldsymbol{\sigma}_1-\boldsymbol{\sigma}_2)/2$, and $F_{np}(r)$ is a short-range function representing the finite size of the neutron charge distribution (for details, see Ref. [16]). Because the S-wave expectation values for the tensor and spin-orbit operators vanish, the long-range $1/r^3$ parts do not contribute for $L=0$. For $L\neq0$, we make the approximation that $\delta^{\rm EM}_{{\rm EM}+N}\approx\delta_N$ (or $S^{\rm EM}_{{\rm EM}+N}\approx S_N$ in terms of the S matrix). This means that in our calculations the asymptotic behavior of the deuteron wave functions still satisfies Eqs. (4.7) and (4.14).

The interaction (4.26) is included only in the case of the Argonne AV18 NN potential [16] where it contributes 18 keV to the deuteron binding energy, mostly from the magnetic moment part $V_{\rm MM}(np)$ of the interaction. One would expect that the inner part of the deuteron wave function is affected by the inclusion or omission of $V_{\rm EM}(np)$ (the outer part is essentially insensitive since it is ruled by γ which is identical for all potentials). Fortunately, it turns out that the quantitative effect is very small, as will be demonstrated below. Thus, also models that do not include the electromagnetic interaction between protons and neutrons can be considered as sufficiently reliable for our study.

Since all NN potentials are fitted to the value of γ given in Eq. (4.20), they all accurately describe the empirical deuteron binding energy, $B_d=2.224\ 575(9)$ MeV [23], via the relativistic relation Eq. (4.17). The other deuteron parameters, as well as the $^3S_1$ scattering length a_t and effective range r_t, are listed in Table I. Predictions are given for the five high-precision NN potentials that we focus on, namely, AV18 [16], CD-Bonn [30], Nijm-I [31], Nijm-II [31], and Reid93 [31]. Notice that not all quantities in Table I are independent. For example, the deuteron effective range $\rho_d\equiv\rho(-B_d,-B_d)$ is related to A_S, η, and γ by

$$A_S^2(1+\eta^2)=\frac{2\gamma}{1-\gamma\rho_d}. \tag{4.28}$$

For our present investigation, essentially only A_S is of relevance (besides γ). However, A_S (and ρ_d) cannot be measured directly. The empirical information given in the last column of Table I on A_S and ρ_d are model-dependent extrapolations of low-energy data. Therefore, to trust the predictions for A_S by our NN potentials, it is important that these models reproduce accurately all measured low-energy data, which is confirmed by Table I. The only exceptions are the deuteron matter radius r_d and the quadrupole moment Q_d, which are both underpredicted by all potential models. There are, however, meson-exchange current contributions and relativistic corrections for r_d and Q_d which may make up for the discrepancies [32,33]. The D-state probability, P_D, that is listed in the bottom row of Table I, is not an observable. It is, however, an interesting theoretical quantity in studies of the nuclear force. The lower value for P_D predicted by CD-Bonn is a reflection of the nonlocal nature of this potential which is based upon relativistic meson field theory [30,34]. Meson-exchange Feynman diagrams are, in general, nonlocal expressions that are represented in momentum space in analytic form.

Finally, in Fig. 1, we display the deuteron wave functions produced by the five NN potential models. Major differences are, again, related to whether the models are local or nonlocal. While the central potentials of AV18, Nijm-II, and

TABLE I. Triplet S-wave low-energy scattering parameters and deuteron properties.

	AV18	CD-Bonn	Nijm-I	Nijm-II	Reid93	Empirical
a_t (fm)	5.419	5.419	5.418	5.420	5.422	5.419(7) [a]
$r_t=\rho(0,0)$ (fm)	1.753	1.752	1.751	1.753	1.755	1.754(8) [a]
$\rho_d=\rho(-B_d,-B_d)$ (fm)	1.767	1.764	1.762	1.764	1.769	1.765(5) [b]
A_S (fm$^{-1/2}$)	0.8850	0.8845	0.8841	0.8845	0.8853	0.8845(9) [b]
η	0.0250	0.0255	0.0253	0.0252	0.0251	0.0256(4) [c]
r_d (fm)	1.967	1.966	1.967	1.968	1.969	1.97535(85) [d]
Q_d (fm^2)	0.270	0.270	0.272	0.271	0.270	0.2859(3) [e]
P_D (%)	5.76	4.83	5.66	5.64	5.70	—

[a]Reference [24].
[b]References [25,26].
[c]Reference [27].
[d]Reference [28].
[e]References [29,25].

Reid93 are stricly local, the Nijm-I central force includes momentum-dependent terms which give rise to nonlocal structures in the equivalent configuration-space potential. This affects the deuteron S wave and is the reason why the $u(r)$ generated by CD-Bonn and Nijm-I are so similar (large solid and dashed curves in Fig. 1) and differ from the other three potentials. The Nijm-I tensor potential is strictly local, similar to AV18, Nijm-II, and Reid93, which explains why these four potentials generate very similar D waves. The CD-Bonn tensor potential is nonlocal.

V. AXIAL ONE-BODY CURRENT CONTRIBUTION

Using the wave functions as defined in Eqs. (2.4) and (2.5) and ignoring the D-wave contribution in the initial scattering state, we find that the matrix element of the (dominant) one-body part of the axial current is given by

$$\langle d,M|A^{(1)}_\mu|pp\rangle=\delta_{M,\mu}\sqrt{16\pi}g_A\frac{e^{i\delta_0}}{k}\int_0^\infty dr\,u(r)\chi_0(r;k)$$
$$\equiv\sqrt{\frac{32\pi}{\gamma^3}}g_A C_0\Lambda(E), \tag{5.1}$$

where $A^{(1)}_{\mu=\pm1,0}$ are the spherical components of $\mathbf{A}^{(1)}$,

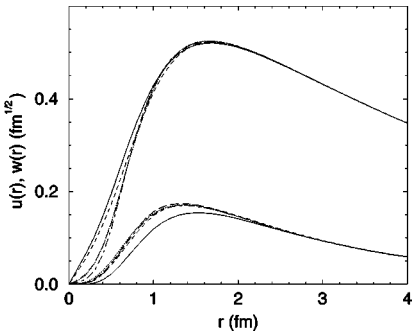

FIG. 1. Deuteron wave functions: large curves, $u(r)$; small curves, $w(r)$. The solid, dashed, dash-dotted, dotted, and long-dashed curves are generated from the CD-Bonn, Nijm-I, Nijm-II, Reid93, and AV18 potentials, respectively.

$A_{\mu=\pm}=\mp(A_x\pm iA_y)/\sqrt{2}$ and $A_{\mu=0}=A_z$, C_0 is the Gamow penetration factor, and the overlap integral is conventionally defined as [2]

$$\Lambda(E)=(\gamma^3/2)^{1/2}\frac{e^{i\delta_0}}{C_0 k}\int_0^\infty dr\,u(r)\chi_0(r;k). \tag{5.2}$$

The constant γ is defined in Eq. (4.20), and the wave function χ_0 is normalized as in Eq. (2.6). Because the solar fusion reaction actually occurs at energies of only a few keV, the phase shift δ_0 is extremely small, and so the exponential $e^{i\delta_0}$ can conveniently be approximated by unity. Note that when we adopt the normalization as advocated by Kamionkowski and Bahcall [5], Eq. (3.17), we find

$$\Lambda(E)=(a_{pp}^2\gamma^3/2)^{1/2}\int_0^\infty dr\,u(r)\overline{\chi}_0(r;k), \tag{5.3}$$

where the scattering length a_{pp} is defined as

$$-\frac{1}{a_{pp}}=\lim_{k\to0}C_0^2 k\cot\delta_0. \tag{5.4}$$

Equation (5.3) coincides with the definition of the overlap integral given by Kamionkowski and Bahcall [5]. However, as stated in our discussion on the pp wave function, it is not at all trivial to calculate the correct scattering length a_{pp} when electromagnetic interactions other than the point-particle Coulomb interaction are present.

In the following, we will present our results for the overlap integral using realistic pp and deuteron wave functions. By realistic we mean that these wave functions were obtained by solving the scattering and bound-state equations using the recent high-precision NN potential models, the parameters of which were fitted to give an almost optimal description of the NN scattering data up to laboratory energies of 350 MeV (i.e., χ^2/data≈1). The five NN models we consider consist of the AV18 Argonne model [16], the CD-Bonn model [30], two Nijmegen models, Nijm-I and Nijm-II [31], and a regularized update of the Reid soft-core potential [31]. The AV18 potential was fitted including all finite-size effects in the full electromagnetic potential of Eq. (3.4), whereas the

TABLE II. Square of the overlap integral $\Lambda(E_{\rm lab})$ at various laboratory energies for the five NN potential models. The zero-energy results are obtained by extrapolating the preceding results.

NN model	Ref.	5 keV	4 keV	3 keV	2 keV	0 keV
AV18	[16]	7.002	6.995	6.987	6.980	6.965
CD-Bonn	[30]	7.022	7.014	7.007	6.999	6.985
Nijm I	[31]	7.002	6.994	6.987	6.979	6.965
Nijm II	[31]	7.008	7.000	6.993	6.986	6.971
Reid93	[31]	7.011	7.003	6.996	6.989	6.974

other four potentials used the point-particle approximation, i.e., $F_C(r)=F_t(r)=F_{ls}(r)=1$ and $F_\delta(r>0)=0$. Furthermore, the AV18 potential is the only model which includes the electromagnetic interaction (4.26) also in the deuteron.

In Table II we show the results for $\Lambda^2(E_{\rm lab})$ ($E=E_{\rm lab}/2$) as calculated from Eq. (5.2). The integral was cut off at $r=50$ fm, which is valid since beyond this distance the deuteron wave function has become extremely small, and so the contribution to the overlap integral becomes negligible. The results are shown for laboratory kinetic energies of 5, 4, 3, and 2 keV, which are extrapolated to define the result at zero energy. For each model we use the deuteron and pp scattering wave functions of that particular model. The dependence on the particular NN model is found to be rather small. Taking the average over all five models we find $\Lambda^2(0)=6.975\pm0.010$. Leaving out the CD-Bonn model, which is quite different from the other models in that it is the only model with nonlocal tensor interactions, we find an even smaller model dependence with $\Lambda^2(0)=6.970\pm0.005$.

We again want to stress that these NN models were fitted including the full electromagnetic potential, and so the wave functions have to be calculated in the presence of this same electromagnetic interaction. Truncating it, for example by only including the standard Coulomb interaction, will modify the wave function and, hence, the overlap integral. In Table III we show the effect on $\Lambda^2(E)$ for different truncations of the electromagnetic part of the interaction. For the nuclear interaction we take the AV18 potential as an example. The other models show a similar trend. We consider four different truncations of the electromagnetic interaction, all for point-particle protons. The effect of V_{C2} is seen to be rather small: neglecting it increases $\Lambda^2(0)$ by only 0.0035, which is a 0.05% effect. The proper inclusion of the vacuum polarization is much more important: neglecting it causes an almost 1% increase.

TABLE III. Square of the overlap integral $\Lambda(E_{\rm lab})$ at various laboratory energies for four different truncations of the electromagnetic interaction (all for point-particle protons). The nuclear interaction is the AV18 potential [16]. The result for the full interaction with finite-size contributions is included for comparison.

$V_{\rm EM}(pp)$	5 keV	4 keV	3 keV	2 keV	0 keV
V_{C1}	7.060	7.051	7.043	7.035	7.019
$V_{C1}+V_{C2}$	7.063	7.055	7.047	7.039	7.023
$V_{C1}+V_{\rm VP}$	6.993	6.985	6.978	6.971	6.956
$V_{C1}+V_{C2}+V_{\rm VP}$	6.996	6.989	6.981	6.974	6.960
Full	7.002	6.995	6.987	6.980	6.965

Finally, for the AV18 potential we can also study the finite-size effects and the effect of $V_{\rm EM}(np)$ in the deuteron calculation. Neglecting the finite-size effects underestimates $\Lambda^2(0)$ by only 0.08%, as shown in the table. Simply removing $V_{\rm EM}(np)$ changes the binding energy to $B_d({\rm trunc})=-2.242\,227$ MeV, and hence the asymptotic behavior of the deuteron wave function. The consequence of this is that $\Lambda^2(0)$ increases by 0.03, almost a 0.5% effect. However, if we first refit the binding energy [i.e., make a modified AV18 potential which does not include $V_{\rm EM}(np)$, but which does have the proper asymptotic deuteron wave function], then the difference in $\Lambda^2(0)$ is only 0.001. Hence, the inclusion of $V_{\rm EM}(np)$ under the restriction that the potential model correctly fit the experimental binding energy has only a small effect on the overlap integral, as we alluded to earlier.

VI. BEYOND THE AXIAL ONE-BODY CURRENT CONTRIBUTION

In this section we review the procedure leading to the experimental determination of the Gamow-Teller (GT) matrix element in tritium β decay, and demonstrate the inability of calculations based on axial one-body currents and realistic wave functions from modern interactions to correctly predict this value. After a brief discussion of the axial two-body current operators, we address the issue of their model dependence by adopting the phenomenological approach of constraining them to reproduce the experimental value of the ^{3}H GT matrix element. We then calculate these two-body current contributions to the pp weak capture, examining in particular the question of how their associated uncertainties affect the pp cross section.

A. Tritium β decay

Evidence for the presence of axial two-body current contributions to weak transitions comes from the β decay of tritium. Its half-life can be expressed as

$$(1+\delta_R)t=\frac{K/G_V^2}{f_V\langle\mathbf{F}\rangle^2+f_A\,g_A^2\langle\mathbf{GT}\rangle^2}, \tag{6.1}$$

where $\delta_R=1.9\%$ is the so-called outer radiative correction, t is the half-life, and f_V and f_A are Fermi functions calculated by Towner, as reported by Simpson [35], to have the values 2.8355×10^{-6} and 2.8505×10^{-6}, respectively. The experimental value for the combination K/G_V^2 is (6146.6 ± 0.6) s, as obtained by Hardy *et al.* [9]. This value is actually 0.15% larger than that used by Simpson [35], (6137.2 ± 3.6) s, in his ^{3}H β-decay analysis. Finally, $\langle\mathbf{F}\rangle$ and $\langle\mathbf{GT}\rangle$ denote the reduced matrix element of the Fermi and GT operators, which in the one-body limit are given by, respectively,

$$\langle\mathbf{F}\rangle=\left\langle{}^3{\rm He}\left\|\sum_i\ \tau_{i,+}\right\|{}^3{\rm H}\right\rangle, \tag{6.2}$$

$$\langle\mathbf{GT}\rangle=\left\langle{}^3{\rm He}\left\|\sum_i\ \boldsymbol{\sigma}_i\tau_{i,+}\right\|{}^3{\rm H}\right\rangle. \tag{6.3}$$

Simpson [35] reports the experimental value (1134.6 ± 3.1) s for the combination $(1+\delta_R)tf_V$. In order to extract

a value for the tritium GT matrix element, it is necessary to calculate the Fermi matrix element. If the trinucleons were pure total $T=1/2$, $M_T=\pm 1/2$ states, then the Fermi matrix element would just be one. However, charge-symmetry breaking (CSB) and charge-independence breaking (CIB) and, more importantly, electromagnetic effects in the nuclear interaction lead to a small correction. In the present study, such a correction is calculated using ^{3}H and ^{3}He wave functions obtained with the correlated-hyperspherical-harmonic (CHH) method [36] from the AV18 two-nucleon interaction (including electromagnetic terms) and the Urbana UIX three-nucleon interaction [37]. We find, neglecting isospin admixtures $T\geqslant 3/2$ (the probability of $T=3/2$ components in ^{3}He has been estimated to be about 0.0016%),

$$\langle \mathbf{F}\rangle^2 \equiv 1-\epsilon = 0.9987. \tag{6.4}$$

The present value for ϵ is about twice that obtained by Saito *et al.* [38] in a (converged) Faddeev calculation based on the older Argonne v_{14} two-nucleon [39] and Tucson-Melbourne (TM) three-nucleon [40] interactions and phenomenological CSB and CIB terms constrained to reproduce the observed mass difference in ^{3}H and ^{3}He. However, the individual binding energies are underpredicted by this Hamiltonian model by about 3%. In contrast, the present AV18/UIX CHH wave functions reproduce the experimental binding energies of both systems within less than 10 keV (incidentally, the variational CHH and ''exact'' Faddeev [41] and Green's function Monte Carlo [42] methods produce trinucleon binding energies all within a few keV of each other). It is unclear at this point whether the difference in ϵ values calculated here and in Ref. [38] is to be ascribed to binding energy effects or to differences in the treatment of the electromagnetic, CSB, and CIB interactions (or both). We note that Simpson uses the value $\epsilon=0.0006$ in line with the estimate of Saito *et al.*

Using the measured half-life, and the values $K/G_V^2=(6146.6\pm 0.6)$ s, $f_A/f_V=1.005\,29$, $\langle \mathbf{F}\rangle^2=0.9987$, and $g_A=1.2654\pm 0.0042$, the ''experimental'' GT matrix element is obtained:

$$\langle \mathbf{GT}\rangle|_{\rm expt}=\sqrt{3}(0.957\pm 0.003), \tag{6.5}$$

where the $\sqrt{3}$ is from a Clebsch-Gordan coefficient.

The experimental GT matrix element is compared with predictions from a number of modern Hamiltonians with various combinations of realistic two- and three-nucleon interactions in Table IV. We also give in Table V the calculated percent probabilities of the S-, S'-, P-, and D-wave components in the ^{3}H wave function [36,41]. A few comments are in order. First, the model Hamiltonians with the TM three-nucleon interaction are all designed to reproduce the experimental ^{3}H binding energy in Faddeev calculations by adjusting the cutoff mass in the TM force [41]. As already pointed out, the two-nucleon interactions employed in the present work are of high precision, and produce fits to pp and np scattering data up to laboratory energies of 350 MeV with a χ^2 per datum in the range 1.03–1.09.

Second, in Table IV we also quote the results obtained using the relation

$$\langle \mathbf{GT}\rangle \simeq \sqrt{3}(P_S+P_D/3-P_{S'}/3), \tag{6.6}$$

TABLE IV. One-body and two-body $\Delta\pi$ contributions to the Gamow-Teller matrix element of tritium β decay, obtained with various combinations of modern two- and three-nucleon interactions in CHH and 42-channel Faddeev calculations, the former for the AV18/UIX model only. The one-body results obtained from Eq. (6.6) are also quoted, while those under the heading ''total'' give the sum of the one-body (first column) and $\Delta\pi$ contributions.

Hamiltonian	One-body	Eq. (6.6)	$\Delta\pi$	Total
AV18	0.924	0.925	0.0507	0.975
AV18/TM	0.925	0.925	0.0546	0.980
AV18/UIX	0.922	0.923	0.0560	0.979
CD-Bonn	0.935	0.935	0.0427	0.977
CD-Bonn/TM	0.937	0.937	0.0435	0.980
Nijm I	0.926	0.927	0.0507	0.977
Nijm I/TM	0.928	0.927	0.0534	0.981
Nijm II	0.926	0.927	0.0504	0.976
Nijm II/TM	0.927	0.927	0.0534	0.981
Reid93	0.925	0.926	0.0514	0.977
Reid93/TM	0.926	0.926	0.0549	0.981

where P_S, P_D, and $P_{S'}$ are the probabilities of the S-, D-, and S'-wave components in the ^{3}H state. Use of such a relation implicitly assumes isospin symmetry—namely, that ^{3}H and ^{3}He form an isodoublet—and also ignores the contribution of P-wave components. However, corrections to Eq. (6.6) appear to be very small, a few parts in a thousand.

Third, the results listed in Table IV indicate that modern interactions lead to predictions for the GT matrix element of tritium in the range $\sqrt{3}\times(0.923-0.937)$, and therefore to an underestimate of the experimental value ranging, in relative terms, from 2.1% for CD-Bonn/TM to 3.7% for AV18/UIX.

B. Axial two-body current model

For the axial two-body current operator we use a slightly expanded version of the conventional π- and ρ-meson ex-

TABLE V. The S-, S'-, P-, and D-state percent probabilities in ^{3}H wave functions. The results for the AV18/UIX model are from Ref. [36].

Hamiltonian	S	S'	P	D
AV18	90.10	1.33	0.066	8.51
AV18/TM	89.96	1.09	0.155	8.80
AV18/UIX	89.51	1.05	0.130	9.31
CD-Bonn	91.62	1.34	0.046	6.99
CD-Bonn/TM	91.74	1.21	0.102	6.95
Nijm I	90.29	1.27	0.066	8.37
Nijm I/TM	90.25	1.08	0.148	8.53
Nijm II	90.31	1.27	0.065	8.35
Nijm II/TM	90.22	1.07	0.161	8.54
Reid93	90.21	1.28	0.067	8.44
Reid93/TM	90.09	1.07	0.162	8.68

TABLE VI. Contributions to the Gamow-Teller matrix element of tritium β decay, obtained with the CHH AV18/UIX trinucleon wave functions. The cutoff masses $\Lambda_\pi = 4.8$ fm^{-1} and $\Lambda_\rho = 6.8$ fm^{-1} are used in the axial two-body operators. The cumulative result is 0.9636. The two-body results obtained by retaining only the contributions of the $T=1$ pairs in tritium are also given (column labeled $T=1$).

	Total	$T=1$
One-body	0.9218	
$\Delta\pi$	0.0560	0.0291
$\Delta\rho$	−0.0213	−0.0111
$\pi\rho$	0.0070	0.0035
πS	0.0044	0.0025
ρS	−0.0043	−0.0021

change model first described by Chemtob and Rho [43]. These are two-body currents associated with excitation of intermediate Δ resonances by π and ρ exchanges, the $\pi\rho$ mechanism, and the contact πNN and ρNN interactions. In the tables, these operators are denoted, respectively, as $\Delta\pi$, $\Delta\rho$, $\pi\rho$, πS, and ρS. Explicit expressions for them are listed in the Appendix for completeness. Here we only note that (i) the (nonlocal) momentum-dependent terms in the π, ρ, and $\pi\rho$ operators are retained in contrast to Ref. [38]; (ii) monopole form factors are included at the πNN and ρNN vertices with cutoff masses Λ_π and Λ_ρ, respectively; and (iii) there is significant uncertainty in the leading $\Delta\pi$ and $\Delta\rho$ contributions, since the N to Δ transition axial coupling is not known [44]. In the model adopted here, the latter is related within the quark model to the nucleon g_A, namely, $g_{N\Delta} = (6\sqrt{2}/5) g_A$.

The present approach consists of using the simplest possible two-body operators that give an adequate description of the longest-range mechanisms and of adjusting the cutoff masses *within a given Hamiltonian model* so as to reproduce the experimental ^{3}H GT matrix element. The contributions due to exchanges of heavier mesons, such as the A_1 [45,46], or renormalizations effects, arising from Δ-isobar admixtures in the nuclear wave functions [44], are neglected. However, in the next subsection it is argued that these approximations are not expected to have an impact in any significant way on the theoretical predictions for the pp weak capture cross section once the two-body current model is constrained to fit the GT matrix element of tritium.

C. Axial two-body current contributions to the pp capture and ^{3}H GT matrix element

In Table VI we quote the contributions to the GT matrix element obtained with the CHH AV18/UIX trinucleon wave functions from the individual components of the axial current operators listed in the Appendix. The small differences between the present results and those reported in Ref. [8] are due to the slightly different values used for Λ_π ($\Lambda_\pi = 4.80$ fm^{-1} in the present work versus $\Lambda_\pi = 4.65$ fm^{-1} in Ref. [8]) and, presumably to a lesser extent, to the fact the older calculations were based on a different Hamiltonian model, consisting of the Argonne v_{14} two-nucleon and Urbana-VIII three-nucleon interactions, which, however, did reproduce the experimental binding energies of the trinucleons in a 34-channel Faddeev calculation [47]. The cumulative value for the calculated GT matrix element is $\sqrt{3} \times 0.964$, about 0.7% larger than experiment. A slight adjustment in the cutoff masses Λ_π and Λ_ρ or $N\Delta$ axial coupling (or both) is thus required to bring theory and experiment into perfect agreement. We will return to this point later, in Sec. VII.

To test the model dependence, we have calculated the leading $\Delta\pi$ contribution with 42-channel Faddeev wave functions obtained from the Hamiltonian models discussed earlier, and the results are listed in Table IV. Both the one-body and $\Delta\pi$ contributions show a strong correlation with the D-state probability in the trinucleon wave functions, which is obviously related to the deuteron D-state probability predicted by the underlying two-nucleon interaction, as is evident from Tables I and V. This correlation is a direct consequence of the dominant contributions due to $T=1$ $^1S_0 \rightleftharpoons T=0$ $^3S_1$-$^3D_1$ ($T=0$ $^3D_1$) transitions for the one-body ($\Delta\pi$) component. This has been verified explicitly by including only the above channels in the Faddeev evaluation of the GT matrix element. As a result, the sum of the one-body and $\Delta\pi$ contributions turns out to be essentially model independent, as indicated in Table IV. Such a conclusion is also expected to hold when the remaining two-body contributions are included. Thus, to reproduce the experimental GT matrix element, a single adjustment of the cutoff masses Λ_π and Λ_ρ or $g_{N\Delta}$ in the axial two-body current operators should suffice for all Hamiltonian models considered.

We now turn to the pp capture. We only quote results, presented in Table VII, corresponding to the AV18 and CD-Bonn interactions. The values calculated with these two models, which give the two extremes for the one-body contribution, 6.966 and 6.992, respectively, at zero energy, are within less than 0.2% when all two-body current contributions are included. Thus, the two-body part of the axial current leads to an increase of the AV18 and CD-Bonn one-body results, amounting, respectively, to 1.6% and 1.1%, consistently with the findings of the earlier study [8].

Having demonstrated the model independence of theoretical predictions for the GT matrix element and pp weak capture cross section, we now want to address the issue of how ambiguities in the axial two-body currents might affect this conclusion. To this end, it is useful to decompose the GT matrix element as

$$\left\langle {}^3\mathrm{He}\left|\sum_{i<j} O_{z,+}(ij)\right|{}^3\mathrm{H}\right\rangle = \left\langle {}^3\mathrm{He}\left|\sum_{i<j} O_{z,+}(ij) P_1^\tau(ij)\right|{}^3\mathrm{H}\right\rangle + \left\langle {}^3\mathrm{He}\left|\sum_{i<j} O_{z,+}(ij) P_0^\tau(ij)\right|{}^3\mathrm{H}\right\rangle, \quad (6.7)$$

where $O_{z,+}$ is the z component of any axial two-body current operator, and $P^\tau_{0,1}$ are projection operators over $T=0$ and 1 two-nucleon states:

$$P_0^\tau(ij) + P_1^\tau(ij) = 1, \quad (6.8)$$

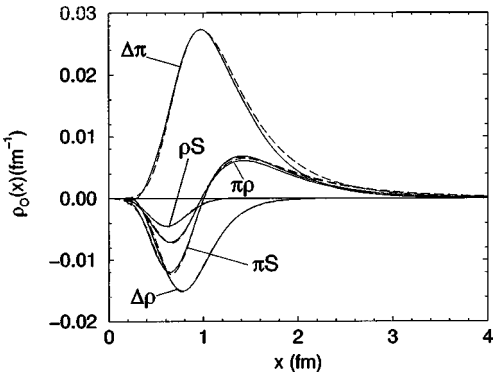

FIG. 2. Gamow-Teller (solid lines) and pp (dashed lines) two-body densities. Note that all pp curves have been rescaled by a single factor, as explained in the text.

$$P_1^\tau(ij)=\frac{3+\boldsymbol{\tau}_i\cdot\boldsymbol{\tau}_j}{4}. \tag{6.9}$$

In Eq. (6.7) most of the $T=0$ ($T=1$) contribution is coming from conversion of a pn $T,S=0,1$ ($nnT,S=1,0$) pair in ^{3}H to a pp $T,S=1,0$ ($pnT,S=0,1$) pair in ^{3}He, for example,

$$\left\langle {}^3\mathrm{He}\left|\sum_{i<j} O_{z,+}(ij)P_1^\tau(ij)\right|{}^3\mathrm{H}\right\rangle \simeq\left\langle {}^3\mathrm{He}\left|\sum_{i<j} P_0^\tau(ij)O_{z,+}(ij)P_1^\tau(ij)\right|{}^3\mathrm{H}\right\rangle, \tag{6.10}$$

since the numbers of $T,S=0,0$ and $T,S=1,1$ pairs in the trinucleons are much smaller than those with $T,S=0,1$ and $T,S=1,0$ [48]. It is now easy to see that, if (neglecting isospin-symmetry breaking corrections) $|{}^3\mathrm{He}\rangle=Q|{}^3\mathrm{H}\rangle$, where $Q\equiv\tau_{1,x}\tau_{2,x}\tau_{3,x}$ is the isospin-flip operator, then

$$\left\langle {}^3\mathrm{He}\left|\sum_{i<j} P_0^\tau(ij)O_{z,+}(ij)P_1^\tau(ij)\right|{}^3\mathrm{H}\right\rangle =\left\langle {}^3\mathrm{He}\left|\sum_{i<j} P_1^\tau(ij)O_{z,+}(ij)P_0^\tau(ij)\right|{}^3\mathrm{H}\right\rangle, \tag{6.11}$$

since the matrix element is real, Q commutes with P_T^τ, $Q^2=1$, and $O_\pm^\dagger=O_\mp$. Thus, the $T=0$ and $T=1$ contributions in Eq. (6.7) are expected to be of about the same size. This can be seen from Table VI, where the sums of the $T=0$ and 1 and $T=1$ alone contributions to the GT matrix element from the individual components of the two-body operators are listed.

It is interesting to define the two-body densities:

$$\rho_O(x;\mathrm{GT})=\left\langle {}^3\mathrm{He}\left|\sum_{i<j}\delta(x-r_{ij})O_{z,+}(ij)P_0^\tau(ij)\right|{}^3\mathrm{H}\right\rangle, \tag{6.12}$$

$$\rho_O(x;pp)=\left\langle pp\left|\sum_{i<j}\delta(x-r_{ij})O_{z,+}(ij)\right|d,0\right\rangle, \tag{6.13}$$

such that

$$\int_0^\infty dx\ \rho_O(x)=O\ \text{ contribution.} \tag{6.14}$$

These densities are shown in Fig. 2, where the $\rho_O(x;pp)$ curves have been rescaled by a *single factor* R, obtained by matching the maximum of the GT and pp $\Delta\pi$ densities. As can be seen from Fig. 2, the GT and pp densities overlap in the region $x\leqslant 2$ fm. Of course, at larger x values the $\rho_O(x;\mathrm{GT})$ is significantly smaller than the $\rho_O(x;pp)$, $O=\pi S,\Delta\pi,\pi\rho$, because of the increased binding in the trinucleons. This scaling is to be expected, since it is a consequence of the ''scaling'' behavior more generally observed for the calculated $T,S=0,1$ and $T,S=1,0$ pair distribution functions in nuclei [48]; see Figs. 3 and 4. Finally, we show in Fig. 5 the $\rho_{\Delta\pi}(x)$ densities obtained with the AV18 and CD-Bonn Hamiltonians for the GT and pp matrix elements. In this case, both the $T=0$ and $T=1$ contributions are included in the GT densities—namely, they have been calculated by removing the isospin projector in Eq. (6.12). Note that the pp densities have been rescaled by a factor $R\simeq 39.0$ obtained by matching the maximum of the AV18 GT and pp densities. However, this rescaling also makes the CD-Bonn GT and pp densities very close (see Fig. 5), demonstrating that the R factor has only a very weak model dependence.

TABLE VII. Square of the overlap integral $\Lambda(E_{\mathrm{lab}})$ at various lab energies for the AV18 and CD-Bonn interactions. The zero-energy results are obtained by linear extrapolation of those at $E_{\mathrm{lab}}=3$ and 5 keV. The cutoff masses $\Lambda_\pi=4.8$ fm^{-1} and $\Lambda_\rho=6.8$ fm^{-1} are used in the axial two-body operators. The two-body contributions are added successively in the given order.

	5 keV		4 keV		3 keV		0 keV	
	AV18	CD-Bonn	AV18	CD-Bonn	AV18	CD-Bonn	AV18	CD-Bonn
One-body	7.002	7.022	6.995	7.014	6.987	7.007	6.965	6.985
$+\pi$S	7.015	7.024	7.007	7.016	6.999	7.009	6.977	6.987
$+\rho$S	7.005	7.018	6.997	7.010	6.990	7.003	6.967	6.981
$+\Delta\pi$	7.138	7.126	7.130	7.118	7.122	7.111	7.099	7.089
$+\Delta\rho$	7.090	7.092	7.083	7.084	7.075	7.077	7.052	7.055
$+\pi\rho$	7.114	7.097	7.107	7.089	7.099	7.082	7.076	7.060

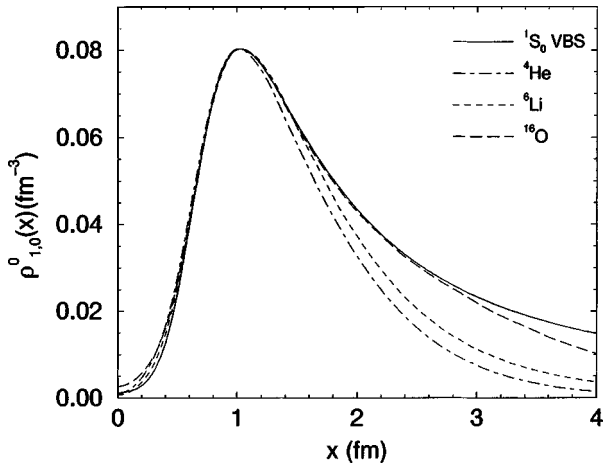

FIG. 3. The $T,S=1,0$ pair distribution functions for various nuclei; see Ref. [48]. Note that the curves have been renormalized to the peak height of the ^{16}O density.

The discussion above shows that two-body contributions to the pp capture are essentially independent of the specific dynamical model adopted as long as the latter is constrained to reproduce the experimental value of the GT matrix element.

VII. CONCLUSIONS

We have calculated the axial matrix element for proton-proton weak capture using five modern high-precision nucleon-nucleon potentials. All these models give excellent fits to elastic NN scattering data with a χ^2/datum near 1 and reproduce measured deuteron properties very well. We have paid particular attention to details of the electromagnetic interaction and the proper treatment of the low-energy pp scattering solutions. As noted before [5] the most important correction to the standard Coulomb interaction between protons is the vacuum polarization, which reduces the cross section by about 1%. We have shown that other fine details of the electromagnetic interaction increase the cross section by about 0.1%. This is in part compensated by the correct relativistic treatment of the deuteron wave number γ, which gives a net 0.03% reduction in the cross section. Including just the axial one-body operator, the five models differ by only 0.3% in the calculated cross section.

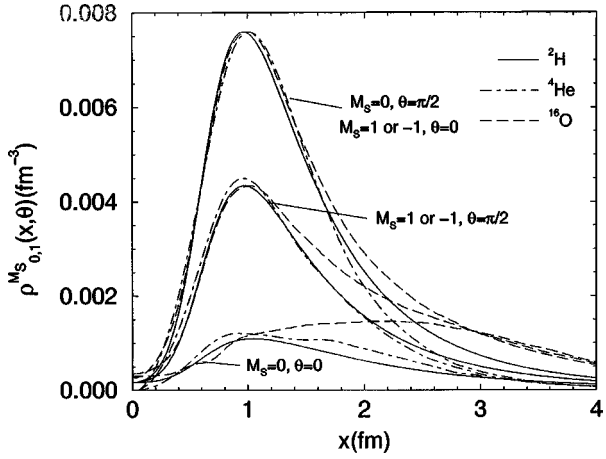

FIG. 4. The $T,S=0,1$ $M_S=0,\pm1$ pair distribution functions for given angles θ between the spin-quantization axis and the relative position vector of the two nucleons and for various nuclei; see Ref. [48]. Note that the curves have been renormalized to the peak height of the deuteron $M_S=\pm1$ $\theta=0$ density.

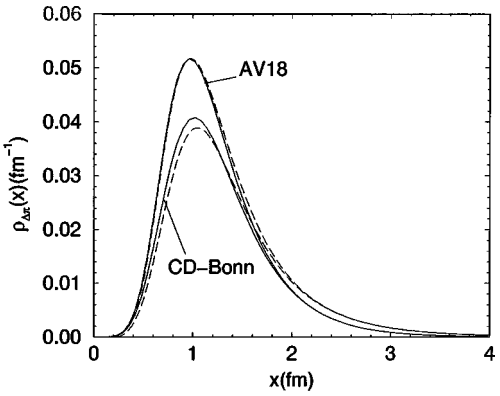

FIG. 5. Gamow-Teller (solid lines) and pp (dashed lines) $\Delta\pi$ densities obtained with the AV18 and CD-Bonn Hamiltonians. Note that the Gamow-Teller densities include both the $T=0$ and $T=1$ contributions—namely, they have been calculated by removing the isospin projector $P^\tau_0(ij)$ in Eq. (6.12). The pp densities have been rescaled by a single factor $R\simeq39.0$, obtained by matching the maximum of the AV18 Gamow-Teller and pp densities.

The biggest remaining uncertainty is in the contribution of axial two-body currents, which can increase the cross section by about 1–1.5 %. Three concerns were expressed at the recent workshop on solar fusion rates [11] regarding the use of the known tritium β-decay rate to predict the axial two-body current contribution to the pp fusion reaction: (1) the model dependence of the one-body contribution to the GT matrix element and the resulting uncertainty in the extracted two-body current contribution to that matrix element; (2) two-body currents coupling $T,T_z=1,0$ pairs to $T,T_z=1,1$ pairs, which can contribute to the tritium GT matrix element but not to the pp capture; and (3) isobar and contact terms could give different contributions to the GT and pp-capture matrix elements, and thus knowledge of their sum in the GT may not be sufficient to predict their sum in the capture matrix element.

Our detailed calculations show that these concerns do not influence the prediction of the pp-capture rate. In particular, (1) the model dependence in the one-body contribution to the GT matrix element comes mostly from that in the D-state probabilities. Because of the smaller D state predicted by the CD-Bonn potential (Table V), the corresponding prediction for this contribution is larger by about 1% (Table IV). However, the prediction obtained with this potential for the pp-capture rate via one-body currents is also larger by about 0.3% (Table II) because of the smaller D state in the deuteron (Table I). The axial two-body currents are necessarily weaker in the CD-Bonn model because they strongly couple the S and D states. In fact the sum of one- and two-body current contributions is much less model dependent than either as can be seen from Tables IV and VII. (2) The axial two-body currents do not couple the $T,T_z=1,0$ pairs to the $T,T_z=1,1$ pairs in any significant way, as the discussion in the preceding section makes clear. (3) The two-body currents are large at small interparticle distances where nuclear forces

dominate over binding energies. In this region the pair wave functions in different nuclei are similar in shape and differ only by a scale factor. This is the basis of the Bethe-Levinger conjecture [49], which can be used to relate processes such as pion and photon absorption, involving nucleon pairs, in different nuclei [48]. Thus the ratios of GT and pp-capture matrix elements of different two-body current terms are nearly the same as can be seen from Fig. 2. Therefore, knowledge of their sum in the GT matrix element is sufficient to predict their sum in the pp-capture matrix element.

Finally, as we have already mentioned, the GT matrix element is slightly overpredicted [$\sqrt{3}\times 0.964$ versus the experimental value $\sqrt{3}\times(0.957\pm 0.003)$]. Reducing the quark-model prediction for the N to Δ axial coupling in the $\Delta\pi$ and $\Delta\rho$ currents by 20% brings theory and experiment into agreement. The resulting CD-Bonn and AV18 values for the square of the pp overlap integral at zero energy are then found to be 7.045 and 7.059, respectively. Predictions for this quantity with other modern interactions are expected to fall in this range. Thus, the model dependence and theoretical uncertainty appear to be at the level of a few parts in a thousand, much smaller than the estimate given in Ref. [11].

ACKNOWLEDGMENTS

Several of the authors visited the National Institute for Nuclear Theory (INT) at the University of Washington in Seattle during the course of this work and benefited from discussions with the participants of the workshop on solar fusion rates and the program on numerical methods for strongly interacting quantum systems. We would like to thank INT for the kind hospitality. The work of J.C. and R.S. is supported by the U.S. Department of Energy; that of V.G.J.S. and R.B.W. is supported by the U.S. Department of Energy, Nuclear Physics Division, under Contract No. W-31-109-ENG-38; that of W.G., H.K., and A.N. is supported by the Deutsche Forschungsgemeinschaft and the Research Contract No. 41324878 (COSY-044) of the Forschungszentrum Jülich; that of R.M. and V.R.P. is supported by the U.S. National Science Foundation via Grant No. PHY96-03097 and Grant No. PHY94-21309, respectively; finally, the work of A.K., S.R., and M.V. is supported by the Italian Istituto Nazionale di Fisica Nucleare. The calculations were made possible by grants of computer time from the National Energy Research Supercomputer Center and Hoechstleitungsrechenzentrum Jülich.

APPENDIX: THE AXIAL TWO-BODY CURRENT OPERATORS

For completeness, we list here the momentum-space expressions for the axial two-body currents used in the present work.
(1) Axial π-exchange Δ-excitation current:

$$\mathbf{A}^{(2)}_{a,ij}(\mathbf{q};\Delta\pi) = -\frac{16}{25}\, g_A\, \frac{f^2_{\pi NN}}{m^2_\pi (m_\Delta - m)}\, \frac{\boldsymbol{\sigma}_j\cdot\mathbf{k}_j}{m^2_\pi + k^2_j}\, f^2_\pi(k_j)[4\ \tau_{j,a}\ \mathbf{k}_j - (\boldsymbol{\tau}_i\times\boldsymbol{\tau}_j)_a\ \boldsymbol{\sigma}_i\times\mathbf{k}_j] + i\rightleftharpoons j. \tag{A1}$$

(2) Axial ρ-exchange Δ-excitation current:

$$\mathbf{A}^{(2)}_{a,ij}(\mathbf{q};\Delta\rho) = \frac{4}{25}\, g_A\, \frac{g^2_\rho (1+\kappa_\rho)^2}{m^2 (m_\Delta - m)}\, \frac{f^2_\rho(k_j)}{m^2_\rho + k^2_j}\{4\ \tau_{j,a}\ (\boldsymbol{\sigma}_j\times\mathbf{k}_j)\times\mathbf{k}_j - (\boldsymbol{\tau}_i\times\boldsymbol{\tau}_j)_a\ \boldsymbol{\sigma}_i\times[(\boldsymbol{\sigma}_j\times\mathbf{k}_j)\times\mathbf{k}_j]\} + i\rightleftharpoons j. \tag{A2}$$

(3) Axial π-exchange (pair) current:

$$\mathbf{A}^{(2)}_{a,ij}(\mathbf{q};\pi S) = \frac{g_A}{2m}\, \frac{f^2_{\pi NN}}{m^2_\pi}\, \frac{\boldsymbol{\sigma}_j\cdot\mathbf{k}_j}{m^2_\pi + k^2_j}\, f^2_\pi(k_j)\{(\boldsymbol{\tau}_i\times\boldsymbol{\tau}_j)_a \boldsymbol{\sigma}_i\times\mathbf{k}_j - i\,\tau_{j,a}[\mathbf{q} + \mathrm{i}\boldsymbol{\sigma}_i\times(\mathbf{p}_i + \mathbf{p}'_i)]\} + i\rightleftharpoons j. \tag{A3}$$

(4) Axial ρ-exchange (pair) current:

$$\begin{aligned}\mathbf{A}^{(2)}_{a,ij}(\mathbf{q};\rho S) = -g_A \frac{g^2_\rho (1+\kappa_\rho)^2}{8m^3}\, \frac{f^2_\rho(k_j)}{m^2_\rho + k^2_j} (&\tau_{j,a}\{(\boldsymbol{\sigma}_j\times\mathbf{k}_j)\times\mathbf{k}_j - i[\boldsymbol{\sigma}_i\times(\boldsymbol{\sigma}_j\times\mathbf{k}_j)]\times(\mathbf{p}_i + \mathbf{p}'_i)\} \\ &+ (\boldsymbol{\tau}_i\times\boldsymbol{\tau}_j)_a\{\mathbf{q}\boldsymbol{\sigma}_i\cdot(\boldsymbol{\sigma}_j\times\mathbf{k}_j) + i(\boldsymbol{\sigma}_j\times\mathbf{k}_j)\times(\mathbf{p}_i + \mathbf{p}'_i) - [\boldsymbol{\sigma}_i\times(\boldsymbol{\sigma}_j\times\mathbf{k}_j)]\times\mathbf{k}_j\}) + i\rightleftharpoons j.\end{aligned} \tag{A4}$$

(5) Axial $\pi\rho$ current:

$$\mathbf{A}^{(2)}_{a,ij}(\mathbf{q};\pi\rho) = -g_A \frac{g^2_\rho}{m}\, \frac{\boldsymbol{\sigma}_j\cdot\mathbf{k}_j}{(m^2_\rho + k^2_i)(m^2_\pi + k^2_j)}\, f_\rho(k_i) f_\pi(k_j)(\boldsymbol{\tau}_i\times\boldsymbol{\tau}_j)_a[(1+\kappa_\rho)\boldsymbol{\sigma}_i\times\mathbf{k}_i - \mathrm{i}(\mathbf{p}_i + \mathbf{p}'_i)] + i\rightleftharpoons j. \tag{A5}$$

Here $\mathbf{q}$ is the total momentum transfer $=\mathbf{k}_i + \mathbf{k}_j$, $\mathbf{k}_{i(j)}$ is the momentum transfer to nucleon i (j), $\mathbf{p}_i$ and $\mathbf{p}'_i$ are the initial and final momenta of nucleon i, and $f_{\pi(\rho)}(k)$ = pion (ρ-meson)-nucleon monopole vertex form factor. The quark model has been used to relate the $\pi N\Delta$, $\rho N\Delta$, and axial $N\Delta$ couplings to, respectively, the πNN, ρNN, and g_A couplings. The expression for πS represents the conventional pair current operator given in the literature. It is obtained with pseudoscalar pion-nucleon coupling. With pseudovector coupling the pion momentum $\mathbf{k}_j$ in the first term in brackets would be replaced by the external momentum $\mathbf{q}$ and an additional term $(\mathbf{p}_i + \mathbf{p}'_i)$ would appear with the isospin structure $(\boldsymbol{\tau}_i\times\boldsymbol{\tau}_j)_a$. Furthermore, the ρS operator includes only those terms which are proportional to $(1+\kappa_\rho)^2$. Finally, m_π, m_ρ, m, and m_Δ are, respectively, the pion, ρ-meson, nucleon, and Δ masses.

[1] H.A. Bethe and C.L. Critchfield, Phys. Rev. **54**, 248 (1938).
[2] E.E. Salpeter, Phys. Rev. **88**, 547 (1952).
[3] J.N. Bahcall and R.M. May, Astrophys. J. **152**, L17 (1969).
[4] R.J. Gould and N. Guessoum, Astrophys. J. **359**, L67 (1990).
[5] M. Kamionkowski and J.N. Bahcall, Astrophys. J. **420**, 884 (1994).
[6] M. Gari and A.H. Huffman, Astrophys. J. **178**, 543 (1972).
[7] F. Dautry, M. Rho, and D.O. Riska, Nucl. Phys. **A264**, 507 (1976).
[8] J. Carlson, D.O. Riska, R. Schiavilla, and R.B. Wiringa, Phys. Rev. C **44**, 619 (1991).
[9] J.C. Hardy, I.S. Towner, V.T. Koslowsky, E. Hagberg, and H. Schmeing, Nucl. Phys. **A509**, 429 (1990).
[10] We use units such that $\hbar = c = 1$.
[11] E. Adelberger *et al.*, Rev. Mod. Phys. (to be published).
[12] Particle Data Group, R. M. Barnett *et al.*, Phys. Rev. D **54**, 1 (1996).
[13] H. Abele *et al.*, Phys. Lett. B **407**, 212 (1997).
[14] *Handbook of Mathematical Functions*, edited by M. Abramowitz and I.A. Stegun (Dover, New York, 1970).
[15] J.R. Bergervoet, P.C. van Campen, W.A. van der Sanden, and J.J. de Swart, Phys. Rev. C **38**, 15 (1988).
[16] R.B. Wiringa, V.G.J. Stoks, and R. Schiavilla, Phys. Rev. C **51**, 38 (1995).
[17] G.E. Bohannon and L. Heller, Phys. Rev. C **15**, 1221 (1977).
[18] G. Breit, Phys. Rev. **99**, 1581 (1955).
[19] E.A. Uehling, Phys. Rev. **48**, 55 (1935).
[20] L. Durand III, Phys. Rev. **108**, 1597 (1957).
[21] L. Heller, Phys. Rev. **120**, 627 (1960).
[22] M.I. Haftel and F. Tabakin, Nucl. Phys. **A158**, 1 (1970).
[23] C. van der Leun and C. Alderliesten, Nucl. Phys. **A380**, 261 (1982).
[24] T.L. Houk, Phys. Rev. C **3**, 1886 (1971); W. Dilg, *ibid.* **11** 103 (1975); L. Koester and W. Nistler, Z. Phys. A **272**, 189 (1975); S. Klarsfeld, J. Martorell, and D.W.L. Sprung, J. Phys. G **10**, 165 (1984).
[25] T.E.O. Ericson and M. Rosa-Clot, Nucl. Phys. **A405**, 497 (1983).
[26] J.J. de Swart, C.P.F. Terheggen, and V.G.J. Stoks, ''The Low-Energy np Scattering Parameters and the Deuteron,'' University of Nijmegen report nucl-th/9509032, 1995.
[27] N.L. Rodning and L.D. Knutson, Phys. Rev. C **41**, 898 (1990).
[28] A. Huber, Th. Udem, B. Gross, J. Reichert, M. Kourogi, K. Pachucki, M. Weitz, and T.W. Hänsch, Phys. Rev. Lett. **80**, 468 (1998).
[29] D.M. Bishop and L.M. Cheung, Phys. Rev. A **20**, 381 (1979).
[30] R. Machleidt, F. Sammarruca, and Y. Song, Phys. Rev. C **53**, 1483 (1996).
[31] V.G.J. Stoks, R.A.M. Klomp, C.P.F. Terheggen, and J.J. de Swart, Phys. Rev. C **49**, 2950 (1994).
[32] J.L. Friar, J. Martorell, and D.W.L. Sprung, Phys. Rev. A **56**, 4579 (1997).
[33] A.J. Buchmann, H. Henning, and P.U. Sauer, Few-Body Syst. **21**, 149 (1996).
[34] R. Machleidt, Adv. Nucl. Phys. **19**, 189 (1989).
[35] J.J. Simpson, Phys. Rev. C **35**, 752 (1987).
[36] A. Kievsky, M. Viviani, and S. Rosati, Phys. Rev. C **52**, R15 (1995).
[37] B.S. Pudliner, V.R. Pandharipande, J. Carlson, and R.B. Wiringa, Phys. Rev. Lett. **74**, 4396 (1995).
[38] T.-Y. Saito, Y. Wu, S. Ishikawa, and T. Sasakawa, Phys. Lett. B **242**, 12 (1990).
[39] R.B. Wiringa, R.A. Smith, and T.L. Ainsworth, Phys. Rev. C **29**, 1207 (1984).
[40] S.A. Coon, M.D. Scadron, P.C. McNamee, B.R. Barrett, D.W.E. Blatt, and B.H.J. McKellar, Nucl. Phys. **A317**, 242 (1979).
[41] A. Nogga D. Hüber, H. Kamada, and W. Glöckle, Phys. Lett. B **409**, 19 (1997).
[42] B.S. Pudliner, V.R. Pandharipande, J. Carlson, S.C. Pieper, and R.B. Wiringa, Phys. Rev. C **56**, 1720 (1997).
[43] M. Chemtob and M. Rho, Nucl. Phys. **A163**, 1 (1971).
[44] R. Schiavilla, R.B. Wiringa, V.R. Pandharipande, and J. Carlson, Phys. Rev. C **45**, 2628 (1992).
[45] S. Ciechanowicz and E. Truhlik, Nucl. Phys. **A414**, 508 (1984).
[46] I.S. Towner, Phys. Rep. **155**, 263 (1987).
[47] C.R. Chen, C.L. Payne, J.L. Friar, and B.F. Gibson, Phys. Rev. C **33**, 1740 (1986); (private communication).
[48] J.L. Forest, V.R. Pandharipande, S.C. Pieper, R.B. Wiringa, R. Schiavilla, and A. Arriaga, Phys. Rev. C **54**, 646 (1996).
[49] J.S. Levinger, *Nuclear Photo-Disintegration* (Oxford University Press, New York, 1960).